ALT 12
Advanced Laser Technologies
2 – 6 September 2012, Thun, Switzerland

ALT 12
c/o Bern University of Applied Sciences
Engineering and Information Technology
Pestalozzistrasse 20, CH-3400 Burgdorf
info@alt12.org, www.alt12.org
0041 (0) 34 426 42 06

MODELING OF NON-EQUILIBRIUM EFFECTS IN SILICON IRRADIATED BY PULSED LASER

Author:

A. Mazhukin

DOI: 10.12684/alt.1.56

Corresponding author: A. Mazhukin

e-mail: specimen@mail.ru

Modeling of non-equilibrium effects in silicon irradiated by pulsed laser

A. Mazhukin

Keldysh Institute of Applied Mathematics of RAS, Moscow, Miusskaya sq.4, Russia

Abstract

In this paper, we use the methods of mathematical modeling to investigate the action of laser pulse (picosecond) with a wave length of $\lambda_L=0.53\mu m$ and the photon energy exceeding the band gap of silicon $\hbar\omega>E_g$ on silicon target. The main feature of these regimes of laser irradiation is strong non-equilibrium of heating and melting processes, which is manifested in a large temperature difference between the carriers and the lattice.

Introduction

Pulsed laser radiation is a widely used tool for precision machining of materials, including semiconductors. Among semiconductor materials, silicon was most widespread in the instrument-making and is one of the most promising materials for thin-film nanotechnology.

To optimize existing and develop new technologies of laser surface treatment of semiconductors it is necessary to perform a detailed study of the dynamics of processes occurring in the irradiation zone and leading to surface modification, including an analysis of the processes of heating, melting and evaporation.

In this paper, we use the methods of mathematical modeling to investigate the action of laser pulse (picosecond) with a wave length of $\lambda_L=0.53\mu m$ and the photon energy exceeding the band gap of silicon $\hbar\omega>E_g$ on silicon target. laser irradiation is strong non-equilibrium of heating and melting processes, which is manifested in a large temperature difference between the carriers and the lattice.

Laser radiation with intensity $G(t)$, Gaussian distribution and wavelength λ_L extending from left to right (Fig. 1) falls on silicon target surface, where the part of the radiation is reflected and some is absorbed. The released energy of laser pulse causes heating, melting (moving boundary Γ_{sl} - melting front) and evaporation (moving boundary Γ_{lv} - evaporation front).

Model

The mathematical model consists of transport equations of the laser radiation, which takes into account the temperature dependence of the reflectivity of the surface, the carrier balance equation that takes into account generation (photo-ionization) and recombination of charged particles (Auger recombination, and photo-recombination), the balance equations of energy carriers and the lattice, taking into account the absorption of laser energy, the exchange of energy between the electron and phonon subsystems, heat and mass transfer [1-2].

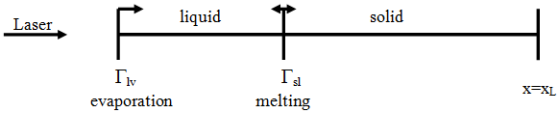

Fig.1. Scheme of laser irradiation.

The basis of first-order phase transitions is the mechanism of heterogeneous melting and evaporation. The process of melting - crystallization is described in approximation of classical variant of Stefan problem and the process of evaporation is described in approximation of Knudsen layer (single-phase version of Stefan problem).

Semiconductor has the properties of metal after melting temperature is reached. And therefore it is necessary to write equations for the solid and liquid regions.

Equations for solid region:

$$\frac{\partial N}{\partial t}=-\frac{\partial J}{\partial x}+I_{en}-R_{en}, \qquad (1)$$

$$\frac{\partial \varepsilon_e}{\partial t}=-\frac{\partial W_e}{\partial x}-\frac{\partial G}{\partial x}-g(T_e)_{lat}(T_e-T_{lat}), \qquad (2)$$

$$\frac{\partial \varepsilon_{lat}}{\partial t}=-\frac{\partial W_{lat}}{\partial x}+g(T_e)_{lat}(T_e-T_{lat}), \qquad (3)$$

$$\frac{\partial G}{\partial x}=-(\alpha+\beta_1)G-\beta_2 G^2, \qquad (4)$$

$$\Gamma_{sl}<x<x_L$$

Equation (1) is equation for a concentration. Equations (2), (3) are energy equations for electron

component and lattice. Equation (4) is equation of laser energy transfer.

Equations for liquid region:

$$\frac{\partial \varepsilon_e}{\partial t} = \frac{\partial}{\partial x}\left(\lambda_e(T_e,T_l)\frac{\partial T_e}{\partial x}\right) - g(T_e)(T_e - T_l) - \frac{\partial G}{\partial x} \qquad (5)$$

$$\frac{\partial \varepsilon_l}{\partial t} = \frac{\partial}{\partial x}\left(\lambda_l(T_l)\frac{\partial T_l}{\partial x}\right) + g(T_e)(T_e - T_l) \qquad (6)$$

$$\frac{\partial G}{\partial x} = -\alpha G, \qquad G(t) = G_0 exp\left(-\left(\frac{t}{\tau}\right)^2\right) \qquad (7)$$

$$\Gamma_{l\upsilon} < x < \Gamma_{sl}$$

Where N – carrier concentration, J – particle current density, ε_e и ε_{lat} – internal energy of electron gas and lattice, W_e и W_{lat} – heat flow of electron gas and lattice, x_L – right end of the sample, λ_e и λ_l – heat conductivity coefficient of electron gas and liquid metal, $I_{en} = \frac{\beta_1 G}{\hbar\omega} + \frac{\beta_2 G^2}{2\hbar\omega} + k_i(T_e)N$ and $R_{en}=\gamma N^3$ – electron-hole pairs generation and recombination velocities, γ - Auger recombination coefficient and ω - laser irradiation frequency, α – free-carrier absorption coefficient, β_1 and β_2 - coefficients of one and two photon absorption, k_i - collision ionization coefficient, $g(T_e)$, $g(T_e)_{lat}$ – electron-lattice energy exchange factor for metal and semiconductor, $g(T_e)_{lat}=C_e/\tau_E$, τ_E - energy relaxation time, C_e – heat capacity. $g(T_e)$ and other thermophysical properties of metals reported in [4]. Equations (5), (6) are energy equations for electron component and lattice one. Equation (7) is equation of laser energy transfer.

Boundary conditions:

$x = x_L$: $\quad J = 0,\ W_e = W_{lat} = 0$

$x = \Gamma_{sl}(t)$: for electron component:

$$(W_e)_s = (W_e)_l,\ (T_e)_s = (T_e)_l,$$

for lattice: $\quad T_s = T_l = T_m,$

$$\left(\lambda_{lat}\frac{\partial T_{lat}}{\partial x}\right)_s - \left(\lambda_{lat}\frac{\partial T_{lat}}{\partial x}\right)_l = \rho_s L_m \upsilon_{sl},$$

$x = \Gamma_{l\upsilon}(t)$: for electron component:

$$J = 0,\ W_e = 0,\ G_l(t) = AG(t)$$

for lattice:

$$\lambda\frac{\partial T_l}{\partial x} = \rho_l L_\upsilon \upsilon_{l\upsilon}$$

$$\rho_l \upsilon_{l\upsilon} = \rho_\upsilon(\upsilon_{l\upsilon} - u)$$

$$P_l + \rho_l \upsilon_{l\upsilon}^2 = P_\upsilon + \rho_\upsilon(\upsilon_{l\upsilon} - u)^2$$

$$T_\upsilon = 0.633T_l, \quad \rho_\upsilon = 0.326\rho_{sat}, \quad u = (\gamma RT_\upsilon)^{1/2}$$

$$\rho_{sat} = \frac{P_{sat}}{RT_l}, \quad P_{sat} = p_b \exp\left[\frac{L_v}{RT_b}\left(1 - \frac{T_b}{T_l}\right)\right]$$

Indexes *lat, l, v, s, sat, b* mean values affiliation to semiconductor lattice, metal liquid phase, vapor, solid phase, saturated vapor and boiling under normal conditions.

Method

Application of the method of dynamic adaptation to the numerical solution of differential equations in partial derivatives allowed determining the spatial and temporal distribution of temperature fields, explicitly distinguishing the position of the moving phase boundary, the speed of its movement, the lifetime of the melt and the thickness of melted and vaporized layers.

Dynamic adaptation method is based on transition to arbitrary non-stationary coordinate system. Following reference [3] we can carry out transition from physical space with Euler variables to calculation space with arbitrary non-stationary coordinate system.

Function characterizing non-stationary coordinate system velocity is not defined and must be found. For definition of this function quasi-stationarity principle was used. It implies that such coordinate system in which $\partial u/\partial\tau=0$ is assumed to be found.

Results

Regimes of irradiation with a Gaussian intensity distribution in the pulse $G(t) = G_0 exp\left(-(t/\tau)^2\right)$ were considered. Pulse duration τ_L = 10 ps. The maximum value of the intensity varied from $G_0=3\text{x}10^9$ to $5\text{x}10^{10}$ W/cm^2. Figures 2 and 3 show the time profiles of temperature and radiation at intensity $G_0 = 3\text{x}10^9$ W/cm^2. It can be seen that at such intensity the gap between the electron temperature and the temperature of the lattice is clearly seen, but the melting does not occur yet.

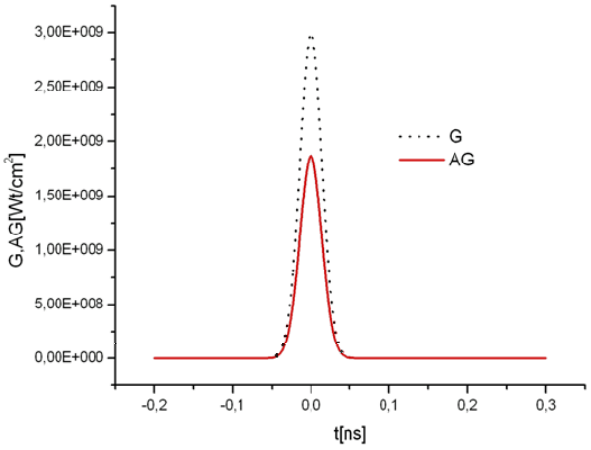

Fig. 2. Time dependences of incident G (black dotted curve) and absorbed part AG (red solid curve) of laser radiation intensity, $G_0=3x10^9$ W/cm^2.

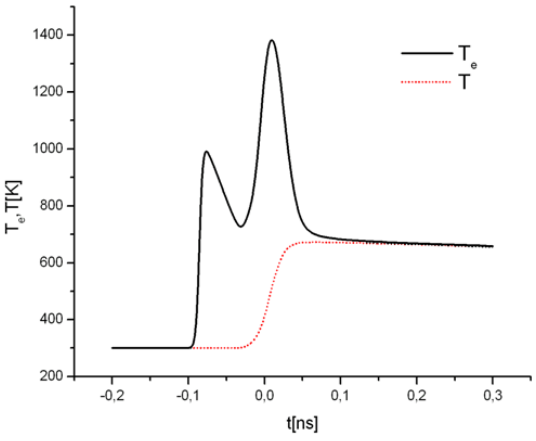

Fig. 3. Time dependences of electron T_e (black solid curve) and lattice (red dotted curve) temperatures.

Increasing the intensity by one order of magnitude leads to the melting of silicon, which starts at the back front of the laser pulse. Typical time profiles of the laser radiation, surface temperatures, melting front velocity and (non)-equilibrium carrier concentrations on the surface for $3x10^{10}$ W/cm^2 energy pulse are shown in Fig. 4-7. Since the melting of lattice starts at the back front of the pulse, the maximum velocity υ_{sl} reaches relatively low value of ~ 27 m/s.

A small change in the intensity of the radiation to $5x10^{10}$ W/cm^2 (Fig. 8-11) leads to the beginning of melting near the maximum of intensity that provides high value of melting velocity υ_{sl} =225 m/s and the gap between temperatures.

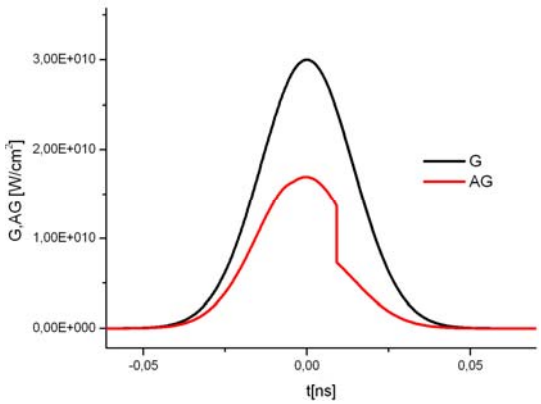

Fig. 4. Time dependences of incident G (black curve) and absorbed part AG (red curve) of laser radiation intensity, $G_0=3x10^{10}$ W/cm^2.

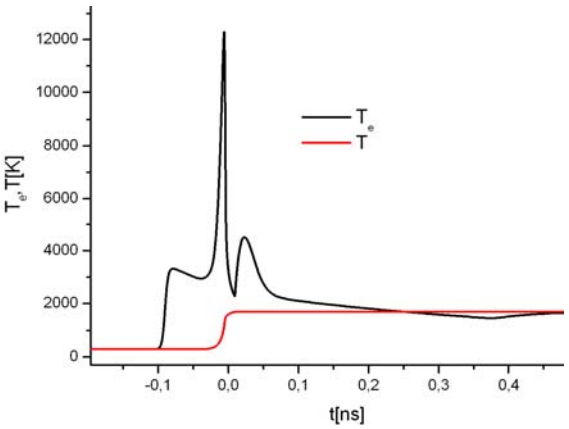

Fig. 5. Time dependences of electron T_e (black curve) and lattice (red curve) temperatures.

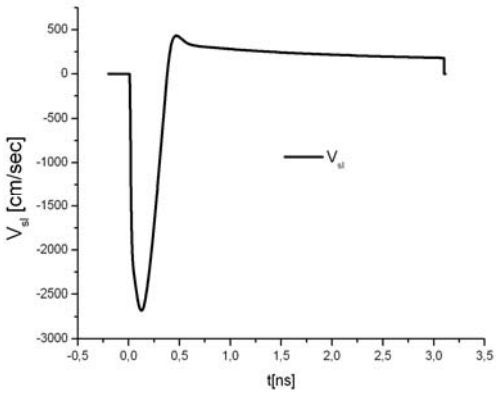

Fig. 6. Time dependence of the melting velocity υ_{sl}.

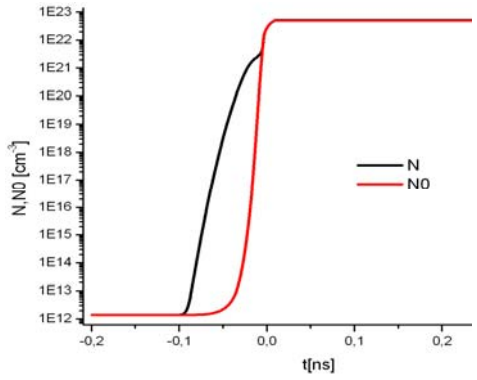

Fig.7. Time dependences of nonequilibrium N (black curve) and equilibrium N_0 (red curve) carrier concentrations on the surface.

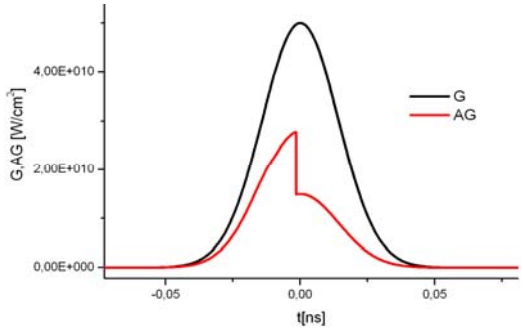

Fig. 8. Time dependences of incident G (black curve) and absorbed part AG (red curve) of laser radiation intensity, G_0=5x10^{10} W/cm^2.

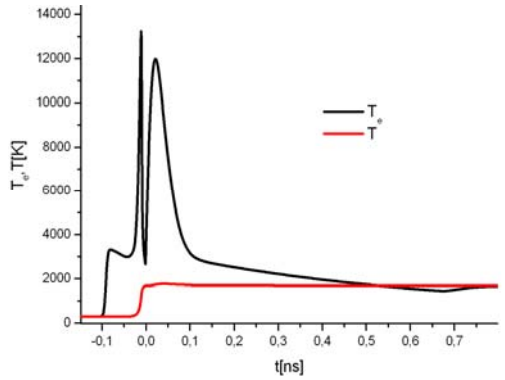

Fig. 9. Time dependences of electron T_e (black curve) and lattice (red curve) temperatures.

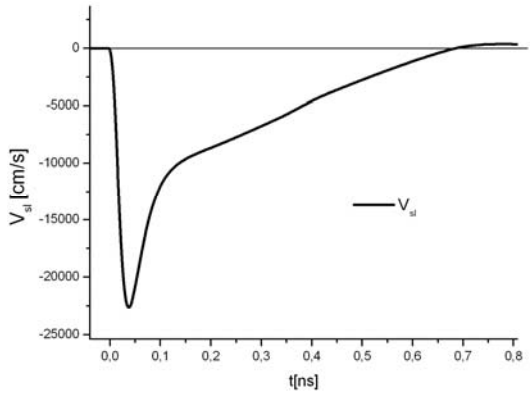

Fig. 10. Time dependence of the melting velocity υ_{sl}.

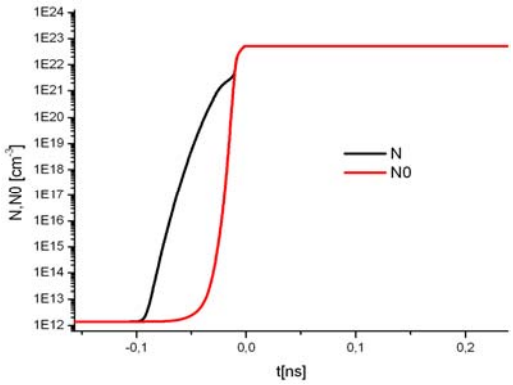

Fig. 11. Time dependences of nonequilibrium N (black curve) and equilibrium N_0 (red curve) carrier concentrations on the surface.

As seen from the time dependences of temperatures (Fig.5 and Fig.9) throughout pulse duration there is a noticeable gap between the phonon and electron temperatures, which reaches 12000K at the peak of the pulse. By the end of the pulse the phonon and electron temperatures become equal.

Maximum melting front velocity reaches 27 m/s for 3x10^{10} W/cm^2 and 225 m/s for 5x10^{10} W/cm^2.

The presence of two peaks in the electron temperature in all regimes of irradiation should be noted, that indicates a change of the mechanism of absorption (photoprocesses replaced by inverse bremsstrahlung).

Acknowledgment. This study was partly supported by RFBR grants 13-07-00597-a, 12-07-00436-a.

References

[1] K. Sokolowski-Tinten, D. von der Linde (2000), "Generation of dense electron hole plasmas in silicon", Phys. Rev. B, 61, pp. 2643-2650.

[2] P. Allenspacher, B. Huttner, W. Riede (2003), "Ultrashort pulse damage of Si and Ge semiconductors", SPIE, 4932, 2003, pp. 358-365.

[3] V.I.Mazhukin, A.V.Mazhukin (2007), "Dynamic adaptation in parabolic equations", Computational Mathematics and Mathematical Physics., vol. 47, 11, pp. 1913-1936.

[4] V.I.Mazhukin (2012), "Kinetics and Dynamics of Phase Transformations in Metals Under Action of Ultra-Short High-Power Laser Pulses", Laser Pulses – Theory, Technology, and Applications Ed. by I. Peshko, Chapter 8, pp-219-276.